Inorganic Chemistry
Article
Cite This: Inorg. Chem. 2019, 58, 10725−10735
pubs.acs.org/IC

Slow Magnetic Relaxation in Dinuclear $Co^{II}Y^{III}$ Complexes

Joydev Acharya,[†] Abinash Swain,[‡] Amit Chakraborty,[†,∥] Vierandra Kumar,[†] Pawan Kumar,[†] Jessica Flores Gonzalez,[§] Olivier Cador,[§] Fabrice Pointillart,*[,§] Gopalan Rajaraman,*[,‡] and Vadapalli Chandrasekhar*[,†,∥]

[†]Department of Chemistry, Indian Institute of Technology Kanpur, Kanpur-208016, India
[‡]Department of Chemistry, Indian Institute of Technology Bombay, Powai, Mumbai-400 076, India
[§]Institut des Sciences Chimiques de Rennes, UMR 6226 CNRS-Université de Rennes 1, 263 Avenue du Général Leclerc, 35042 Rennes Cedex, France
[∥]Tata Institute of Fundamental Research, Gopanpally, Hyderabad-500107, India

Supporting Information

ABSTRACT: Four new dinuclear complexes, $[Co(\mu\text{-L})(\mu\text{-}CCl_3COO)Y(NO_3)_2]\cdot 2CHCl_3\cdot CH_3CN\cdot 2H_2O$ (**1**), $[Co(\mu\text{-L})(\mu\text{-}CH_3COO)Y(NO_3)_2]\cdot CH_3CN$ (**2**), $[Co(\mu\text{-L})(\mu\text{-PhCOO})Y(NO_3)_2]\cdot 3CH_3CN\cdot 2H_2O$ (**3**), and $[Co(\mu\text{-L})(\mu\text{-}^t BuCOO)Y(NO_3)_2]\cdot CHCl_3\cdot 2H_2O$ (**4**), having a $Co^{II}Y^{III}$ core, have been synthesized by employing a ferrocene based compartmental ligand which was synthesized by the reaction of diacetyl ferrocene with hydrazine hydrate followed by a condensation reaction with o-vanillin. A general synthetic protocol was employed to synthesize complexes **1**−**4**, where the metallic core was kept the same with changing the bridging carboxylate groups. In all the complexes, the main structural motif is kept similar by only slightly varying the substitution on the bridging acetate groups. This variation has resulted in a small but subtle influence on the magnetic relaxation of all these four compounds. *Ab initio* CASSCF/NEVPT2 calculations were carried out to assess the effect of the different substitutions of the bridging ligands on the magnetic anisotropy parameters and on orbital arrangements. *Ab initio* calculations yield a very large positive D value, which is consistent with the geometry around the Co^{II} ion and easy plane anisotropy (g_{xx}, $g_{yy} > g_{zz}$), with the order of the calculated D in the range of 72.4 to 91.7 cm^{-1} being estimated in this set of complexes. To ascertain the sign of zero-field splitting in these complexes, EPR spectra were recorded, which support the sign of D values estimated from *ab initio* calculations.

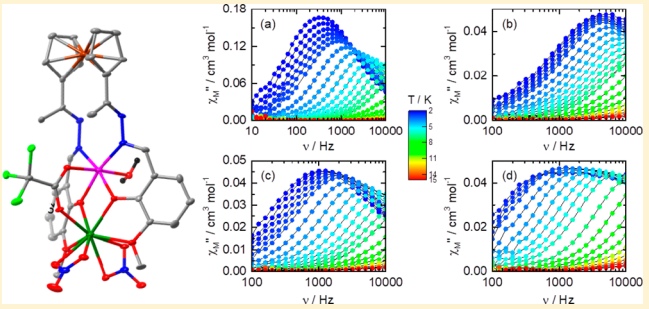

INTRODUCTION

Single-molecule magnets (SMMs), single-ion magnets (SIMs), and single-chain magnets (SCMs) are families of molecular magnets that seem to have considerable promise as materials of the future in applications as diverse as data storage to quantum computing.[1] While it is true that realization of even some of these applications can only be attempted after major challenges in this field are overcome, research in this area continues to grow unabated, driven by an academic interest. One of the qualitative understandings that has emerged as a result of investigations over the past two decades is that in order for a molecule to exhibit the phenomenon of SMM behavior, it should possess a large ground state spin and a large magnetic anisotropy such that a bistable ground state, with an energy barrier equal to $|D|S^2$ for integer spin values and $|D|S^2 - 1/4$ for noninteger spins values, can result (S is total spin and D, a second-order axial anisotropy parameter having value <0). The negative sign of D is an important parameter for assembling good SMMs because it favors high $|m_s|$ states as the ground state. Thus, several complexes have been reported where the value of the axial zero field splitting parameter was negative ($D < 0$), and they were found to be good SMMs with slow magnetic relaxation.[2] In contrast, when $D > 0$, the ground state will be $|m_s| = 0$ for systems with integer S and $|m_s| = \pm 1/2$ Kramer's doublet for those with noninteger S. In this case, it seems that a system with $D > 0$ should have no energy barrier for spin reversal, as the spin is free to rotate within its easy plane. Interestingly, slow magnetic relaxation has also been observed in systems with an easy plane anisotropy ($D > 0$).[3] This fact can be explained by the presence of the rhombic zero-field splitting, *i.e.*, in plane anisotropy given by an $E(S_x^2 - S_y^2)$ term where E is the second-order rhombic anisotropy parameter and whose value is limited to $0 < E/|D| < 0.33$. For high positive D values, the ground state is well separated from the excited state manifolds of the spin multiplets that are not thermally accessible. In such cases, the direct relaxation process and two-phonon Raman process becomes significant

Received: March 26, 2019
Published: August 1, 2019

DOI: 10.1021/acs.inorgchem.9b00864
Inorg. Chem. 2019, 58, 10725−10735

over the Orbach process of the magnetic relaxation. In 2014, Ruiz and colleagues reported an extensive theoretical study on a model complex of Co^{II}, $[Co(acac)_2(H_2O)_2]$ (acac = acetylacetonate) having $D > 0$, and stated that slow relaxation of magnetization naturally occurs following Kramer's theorem, irrespective of the sign of D.[4] Co^{II} being a Kramers ion ($S = 3/2$) is thus a good choice for assembling complexes that can be potential SMMs. We reported the first example of a Co^{II}–Ln^{III}-based SMM, $[LCo^{II}–Gd^{III}–Co^{II}L]^+$ (LH_3 = (S)P[N(Me)N = CH-C_6H_3-2-OH-3-OCH_3]$_3$, a cationic trinuclear complex several years ago.[5] This was followed by other examples of Co^{II}–Ln^{III}-based SMMs.[4,6] A couple of examples of Co^{II}–Y^{III} complexes where Co^{II} is the only paramagnetic center, with a diamagnetic Y^{III} metal ion as the neighbor, have been reported to act as single ion magnets (SIMs).[7] The oxygen bridged diamagnetic metal center not only increases the electron density on the bridged oxygen atom, thereby influencing the electronic environment around the paramagnetic metal center, but also provides a diamagnetic surrounding that may help to prevent the intermolecular spin–spin interaction, increasing the efficiency of single ion magnet behavior. This hypothesis has been tested in some 3d/4f complexes where the 3d metal ion is diamagnetic.[8] On the other hand, examples of 3d/4f complexes where the 3d metal ion is paramagnetic and the adjoining metal ion is diamagnetic are still sparse. There are a few Co^{III}–Co^{II} complexes where this phenomenon has been realized.[9]

Recently, we have designed a ferrocene-supported ligand, LH_2{LH_2 = Fe[(C_5H_4){-C(Me)=N–N=CH-C_6H_3-2-OH-3-OCH_3}]$_2$}, that allowed us to assemble dinuclear 3d/4f complexes.[10] We were interested in examining if this ligand would be amenable to constructing Co^{II}–Y^{III} complexes. Accordingly, four complexes $[Co(\mu\text{-L})(\mu\text{-RCOO})Y(NO_3)_2]$ (Scheme 1) were prepared where a bridging carboxylate group between the Co^{II} and the Y^{III} center is systematically varied [$RCOO^-$ = CCl_3COO^- for **1**; CH_3COO^- for **2**; $PhCOO^-$ for **3**; $^tBuCOO^-$ for **4**, respectively]. In the following, we report the synthesis, structure, magnetism, and theoretical studies on these complexes.

Scheme 1. Synthesis of Complexes 1–4

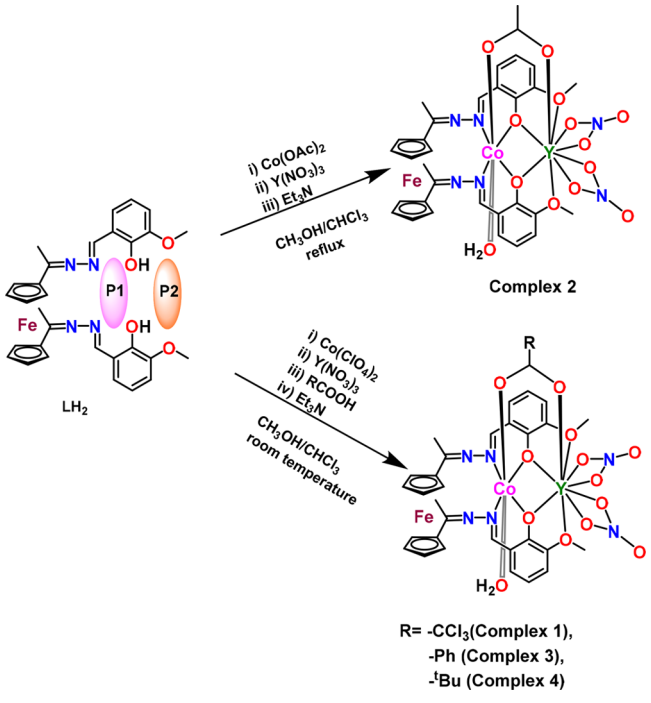

Experimental Section. All the solvents were purified by adopting standard procedures.[11] Acetyl chloride (Spectrochem, Mumbai), ferrocene (Sigma-Aldrich, USA), aluminum chloride, hydrazine hydrate (Spectrochem, Mumbai, India), *o*-vanillin, pivalic acid, benzoic acid, trichloroacetic acid (SD Fine Chemicals, Mumbai, India), $Co(OAc)_2{\cdot}4H_2O$, $Y(NO_3)_3{\cdot}xH_2O$, and $Co(ClO_4)_2{\cdot}6H_2O$ (Sigma-Aldrich, USA) were used as purchased. Diacetylferrocene and 1,1′-diacetylferrocene dihydrazone were synthesized and purified according to reported procedures.[10]

Caution! We did not encounter any problems during our studies; nevertheless, perchlorate salts are potentially explosive and should be handled in small quantities and with care.

Instrumentation. Melting points were measured using a JSGW melting point apparatus and are uncorrected. IR spectra were recorded as KBr pellets on a Bruker Vector 22 FT IR spectrophotometer operating at 400–4000 cm^{-1}. ^1H NMR spectra were recorded on a JEOL JNM LAMBDA 400 model spectrometer operating at 500 MHz. Chemical shifts are reported in parts per million (ppm) and are referenced with respect to internal tetramethylsilane (^1H). Elemental analyses of the compounds were obtained from Thermoquest CE instruments CHNS-O, EA/110 model. Electrospray ionization mass spectrometry (ESI-MS) spectra were recorded on a Micromass Quattro II triple quadrupole mass spectrometer. Methanol was used as the solvent for the electrospray ionization (positive ion, full scan mode). Capillary voltage was maintained at 2 kV, and cone voltage was kept at 31 kV. Variable-temperature EPR spectra of compounds **2–4** in powder were recorded at 5 K and 10 K using a Bruker spectrometer operating at the Q-band (35 GHz) frequency, and the EPR simulation was performed with Easyspin software (version 5.0.0). The dc magnetic susceptibility measurements were performed on solid polycrystalline samples (the microcrystallites were immobilized in pellets) with a Quantum Design MPMS-XL SQUID magnetometer between 2 and 300 K in an applied magnetic field of 2 kOe in the 2–20 K temperature range and 10 kOe above 20 K. All the measurements were corrected for the diamagnetic contribution as calculated with Pascal's constants. The ac magnetic susceptibility measurements were performed on both Quantum Design MPMS-XL SQUID and Quantum Design PPMS magnetometers.

X-ray Crystallography. The SCXRD data for the compounds have been collected on a Bruker SMART CCD diffractometer (Mo$K\alpha$ radiation, λ = 0.71073 Å). Collecting frames of data, indexing reflections, and determining lattice parameters was done by the program SMART; integrating the intensity of reflections and scaling was done by SAINT,[12] SADABS[13] for absorption correction, and SHELXTL[14] for space group and structure determination and least-squares refinements on F^2. The crystal structures were solved and refined by full-matrix least-squares methods against F^2 by using the program SHELXL-2014[15] using Olex^2 software.[16] Some solvent molecules in **1** and **4** have been found to be highly disordered and have weak residual Q peaks. These were masked using Olex^2 program. The void volumes and the possible masked out electron counts have been included in the corresponding CIFs. All other non-hydrogen atoms were refined with anisotropic displacement parameters. The

DOI: 10.1021/acs.inorgchem.9b00864
Inorg. Chem. 2019, 58, 10725–10735

positions of the hydrogen atoms were fixed at calculated positions and refined isotropically thoroughly. The crystallographic figures have been generated using the Diamond 3.1e program.[17] The crystal data and the cell parameters for compounds **1**−**4** are summarized in Table S4.

Computational Details. All calculations were performed on the X-ray structure, and the spin Hamiltonian parameters were calculated using the CASSCF/NEVPT2 approach. We also compared our results with CASSCF/RASSI-SO/SINGLE_ANISO calculations. For this, we have used ORCA 4.0 and the MOLCAS 8.0 suite of programs.[18] Using the ORCA suite, state averaged complete-active space self-consistent field (CASSCF) wave functions were complemented by N electron valence second order perturbation theory (NEVPT2) to assess the role of dynamic correlation. The active space for the CASSCF involves seven d electrons of the five 3d orbitals [CAS(7,5)]. For our calculations, we have computed 10 quartet and 40 doublet states. The polarized triple-ζ quality of the DKH type basis set [DKH-def2-TZVP] was used for Co and Fe, whereas for Y, [Sapporo-DKH3-DZP-2012] was used; for C, N, O, and Cl, DKH-def2-TZVP(-f) was used; and for H, DKH-def2-SVP was used. For the CASSCF step, we have used TrafoStep RIMO approximation and for NEVPT2 RI-NEVPT2 approximation was utilized to speed up the calculations. The spin−orbit coupling was taken into account through the QDPT approaches, and for the ZFS and g tensors, the effective Hamiltonian approach was employed.[19] For the MOLCAS calculations same CAS space and roots were used as mentioned earlier for the ORCA calculations. The basis sets used were of the ANO RCC type with triple-ζ polarization: for carbon, C.ANO-RCC···4s3p2d, H.ANO-RCC···2s, O.ANO-RCC···3s2p1d, N.ANO-RCC···3s2p1d; cobalt, Co.ANO-RCC···6s5p3d2f1g; yttrium, Y.ANO-RCC···7s6p4d2f1g. The magnetic properties were obtained from the SINGLE_ANISO module.[20]

Synthesis. The ligand (H_2L) was synthesized by following a previously published method.[10]

Preparation of Complexes 1, 3, and 4. A general procedure for the synthesis of the complexes **1**, **3**, and **4** is as follows. LH_2 (0.053 mmol) was placed in a chloroform−methanol (30 mL, v/v, 1:1) mixture. To this, $Co(ClO_4)_2\cdot 6H_2O$ (0.053 mmol) was added and stirred for 10 min followed by the addition of $Y(NO_3)_3\cdot xH_2O$ (0.053 mmol) and then Et_3N (0.159 mmol). After stirring for another 10 min, the corresponding acid, RCOOH (0.053 mmol), was added, and the final solution was stirred for the next 8 h at room temperature. Removal of the solvent afforded a reddish solid which was washed by Et_2O followed by redissolution in CH_3CN−$CHCl_3$ (20 mL, v/v, 1:1), which produced suitable crystals for SCXRD upon slow evaporation.

Preparation of Complex 2. To a (30 mL, v/v, 1:1) chloroform−methanol solution of LH_2 (0.053 mmol) was added Et_3N (0.106 mmol) followed by $Y(NO_3)_3\cdot xH_2O$ (0.053 mmol), and the solution was stirred for 10 min. After this, $Co(OAc)_2\cdot 4H_2O$ (0.053 mmol) was added at once, and the solution heated to reflux for 3 h before the solvent was completely stripped off in vacuo, resulting in a red powder which was washed by Et_2O. Single crystals suitable for SCXRD were obtained by slow evaporation after dissolving the red powder in CH_3CN−$CHCl_3$ (20 mL, v/v, 1:1). Specific details of all corresponding reactions' yield and the characterization data of the complexes are given below.

*$[Co(\mu\text{-}L)(\mu\text{-}CCl_3COO)Y(NO_3)_2]\cdot 2CHCl_3\cdot CH_3CN\cdot 2H_2O$ (**1**).* Quantities: LH_2 (0.03g), $Y(NO_3)\cdot 6H_2O$ (0.0203 g), $Co(ClO_4)_2\cdot 6H_2O$ (0.0195 g), CCl_3COOH (0.008 g), Et_3N (0.0161 g), yield: 0.038 g, 53.5% (based on Co^{II}). M.P. > 260 °C. FT-IR (KBr) cm^{-1}: 3388 (b), 2942 (w), 1656 (s), 1606 (s), 1595 (s), 1511 (s), 1476 (s), 1361 (s), 1294 (s), 1220 (s), 842 (s), 742 (s). Anal. Calcd for $C_{36}H_{40}Cl_9CoFeN_7O_{15}Y$ (1333.502): C, 32.42; H, 3.02; N, 7.35. Found: C, 32.68; H, 3.17; N, 7.54.

*$[Co(\mu\text{-}L)(\mu\text{-}CH_3COO)Y(NO_3)_2]\cdot CH_3CN$ (**2**).* Quantities: LH_2(0.03g), $Y(NO_3)\cdot 6H_2O$ (0.0203 g), $Co(OAC)_2\cdot 4H_2O$ (0.013 g), Et_3N (0.0106 g), yield: 0.0289 g, 58% (based on Co^{II}). M.P. > 260 °C. FT-IR (KBr) cm^{-1}: 3374 (b), 2936 (w), 2836 (w), 1668 (w), 1607 (s), 1464 (s), 1384 (s), 1297 (s), 1270 (s), 1219 (s). Anal. Calcd for $C_{34}H_{37}CoFeN_7O_{13}Y$ (955.381): C, 42.74; H, 3.90; N, 10.26. Found: C, 42.68; H, 3.57; N, 10.54.

*$[Co(\mu\text{-}L)(\mu\text{-}PhCOO)Y(NO_3)_2]\cdot 3CH_3CN\cdot 2H_2O$ (**3**).* Quantities: LH_2 (0.03g), $Y(NO_3)\cdot 6H_2O$ (0.0203 g), $Co(ClO_4)_2\cdot 6H_2O$ (0.0195 g), PhCOOH (0.007 g), Et_3N (0.0161 g), yield: 0.0299 g, 49.5% (based on Co^{II}). M.P. > 260 °C. FT-IR (KBr) cm^{-1}: 3388 (b), 2947 (w), 1607 (s), 1554 (s), 1467 (s), 1401 (s), 1297 (s), 1238 (s), 1220 (w). Anal. Calcd for $C_{43}H_{49}CoFeN_9O_{15}Y$ (1135.585): C, 45.48; H, 4.35; N, 11.1. Found: C, 45.68; H, 4.57; N, 11.04.

*$[Co(\mu\text{-}L)(\mu\text{-}^tBuCOO)Y(NO_3)_2]\cdot CHCl_3\cdot 2H_2O$ (**4**).* Quantities: LH_2 (0.03g), $Y(NO_3)\cdot 6H_2O$ (0.0203 g), $Co(ClO_4)_2\cdot 6H_2O$ (0.0195 g), $^tBuCCOOH$ (0.005 g), Et_3N (0.0161 g), yield: 0.0335 g, 56.5% (based on Co^{II}). M.P. > 260 °C. FT-IR (KBr) cm^{-1}: 3372 (b), 3124 (w), 2959 (w), 2320 (w), 1609 (s), 1559 (s), 1473 (s), 1423 (s), 1294 (s), 1238 (s), 1216 (s), 970 (s), 738(s). Anal. Calcd For $C_{36}H_{45}Cl_3CoFeN_6O_{15}Y$ (1111.817): C, 38.89; H, 4.08; N, 7.57. Found: C, 38.61; H, 4.17; N, 7.24.

RESULTS AND DISCUSSION

Synthesis. We have previously demonstrated the utility of ferrocene-supported ligands for the preparation of heterometallic 3d/4f complexes where the ferrocene-based compartmental hexadentate LH_2 ligand is comprised of two specific coordination pockets, an inner coordination pocket (P1, Scheme 1) composed of two imine nitrogen and two bridging phenoxy oxygens (N_2O_2) which specifically bind with 3d ions and an outer coordination pocket (P2, Scheme 1) consisting of two phenoxy oxygens and two methoxy oxygen atoms (O_4 coordination environment) which preferentially bind to 4f metal ions. Thus, utilizing these features of the ligand, previously we reported a set of dinuclear Ni^{II}−Ln^{III} complexes.[10] This time, the reaction of LH_2 with $Co(OAc)_2\cdot 4H_2O$ and $Y(NO_3)_3\cdot xH_2O$ in the presence of Et_3N as a base in a molar ratio of 1:1:1:2 under reflux conditions yields the complex $[Co(\mu\text{-}L)(\mu\text{-}CH_3COO)Y(NO_3)_2]\cdot CH_3CN$ (**2**); here, the acetate ion acts as the bridging ligand linking the Co^{II} and Y^{III} metal ions. Under approximately similar reaction conditions, the reaction of LH_2 with $Co(ClO_4)_2\cdot 6H_2O$ and $Y(NO_3)_3\cdot xH_2O$ in the presence of trichloroacetic acid, benzoic acid, or pivalic acid and Et_3N as the base in a stoichiometric ratio of 1:1:1:1 afforded the complexes $[Co(\mu\text{-}L)(\mu\text{-}CCl_3COO)Y(NO_3)_2]\cdot 2CHCl_3\cdot CH_3CN\cdot 2H_2O$ (**1**), $[Co(\mu\text{-}L)(\mu\text{-}PhCOO)Y(NO_3)_2]\cdot 3CH_3CN\cdot 2H_2O$ (**3**), and $[Co(\mu\text{-}L)(\mu\text{-}^tBu_3COO)Y(NO_3)_2]\cdot CHCl_3\cdot 2H_2O$ (**4**) respectively (Scheme 1). All the complexes possess a similar type of core

DOI: 10.1021/acs.inorgchem.9b00864
Inorg. Chem. 2019, 58, 10725−10735

and only differ in the number/nature of solvent molecules of crystallization.

For investigating the structural integrity of **1**−**4** in solution, we have carried out ESI−MS studies which revealed parent ion peaks for corresponding complexes, although in lower abundance relative to other fragments. A representative ESI-MS spectrum of **1** is given in Figure 1, while spectra for the rest

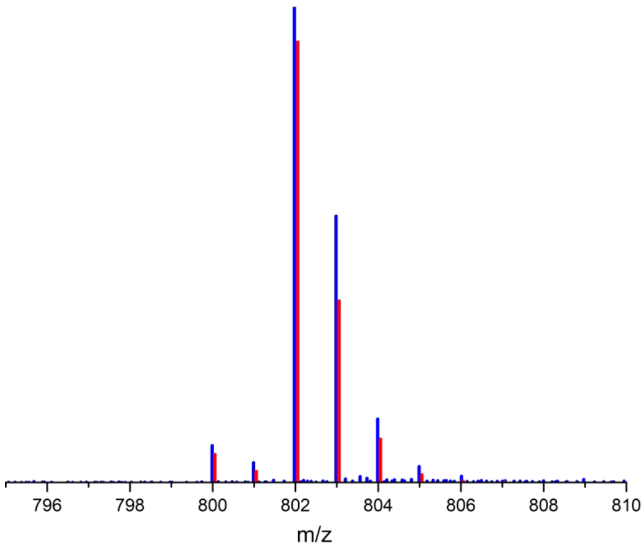

Figure 1. ESI-MS of $[Co(\mu\text{-L})Y(OEt)_2]^+$ (fragment) theoretical simulation (red lines) and experimental spectrum (blue lines) for complex **1**.

of the complexes are given in the Supporting Information. Interestingly, all the complexes, **1**−**4**, show a distinct peak with very high abundance at around m/z = 802. This is presumably due to the common dinuclear fragment, $[Co(\mu\text{-L})Y(OEt)_2]^+$, independent of the nature of the bridging ligand present in these complexes.

X-ray Crystallography. Among the four heterometallic dinuclear $Co^{II}Y^{III}$ complexes, **1**, **2**, and **4** crystallized in the triclinic $P\bar{1}$ space group, while complex **3** crystallized in the monoclinic $P2_1/c$ space group. In view of the structural similarity of the complexes, **2** is taken as a representative example to describe the structural features of this dinuclear complex family.

In complex **2**, the Co^{II} center occupies the inner coordination pocket P1 of the ligand with a 2N−4O coordination environment (see Figure 2 and Scheme 1). The coordinating atoms involved are as follows: two nitrogen atoms, N1 and N2, from the imine part of the ligand [Co−N1, 2.162(3) Å; Co−N2, 2.109(3) Å]; two phenoxide oxygen atoms O4 and O5 of the ligand [Co−O4, 2.062(2) Å; Co−O5, 2.083(2) Å]; one oxygen atom O1 from the bridging carboxylate ligand [Co−O1, 2.032(2) Å]; and finally O3 from the water molecule [Co−O3, 2.123(2) Å]. The overall coordination geometry around Co^{II} can be described as distorted octahedral geometry. The coordination environment around Y^{III} is 9O, and the coordination geometry can be described by continuous SHAPE analysis[21] to be Muffin-shaped (MFF-9) in *Cs* symmetry or, in other words, distorted tricapped trigonal prismatic geometry (Figure 2d). The Y^{III} ion is ensconced in the outer coordination pocket P2 of the ligand. Total coordination arrangement around the Y^{III} ion occurs in the following manner: two bridging phenoxide oxygen atoms O4 and O5 [Y−O4, 2.282(2) Å; Y−O5, 2.083(2) Å]; one oxygen atom O2 from the bridging carboxylate group [Y−O2, 2.284(2) Å]; four oxygen atoms O7, O8, O9, and O10 from two chelating nitrate groups [Y−O7, 2.438(2) Å; Y−O8, 2.478(2) Å; Y−O9, 2.399(2) Å; Y−O10, 2.435(3) Å]; and two oxygen atoms O6 and O11 from two methoxy groups of the ligand [Y−O6, 2.533(2) Å; Y−O11, 2.606(2) Å].

The phenoxide bridging action between the Co^{II} and Y^{III} centers results in a $CoYO_2$ four-membered ring (see Figure S6). Within this ring, it is interesting to note that the two Y−O−Co bridging angles (Co−O4−Y and Co−O5−Y) are not the same in all the complexes. Also, it is worth mentioning that the O4−Co−O5 angle is always greater than the O4−Y−O5 angle for each complex.

As the natures of the bridging carboxylate groups are different in each complex, in spite of the overall structural similarity, certain small but subtle differences are noticed in the four complexes. The obtained CShM values from continuous SHAPE measurement[21] for the OC6↔TPR6 deformation pathway show that the structures are much closer to the OC6 geometry (Table 1) and reveal that the degree of distortion continuously increases from **1** to **4** regularly.

The differences in crystallographic parameters around the Co^{II} center that are summarized in Table 2 also act in support of the difference in distortion from perfect geometry among the complexes.

In three-dimensional arrangements within the crystal structure, two neighboring molecules are seen to have two noncovalent "OH−N" type hydrogen bondings. The hydrogen atoms (H1A, H1B) of coordinated H_2O molecule are in a hydrogen bonding interaction with the two imine N atoms (N2, N4) in the ligand of the adjacent molecule (Figure 2C).

Colacio et al. previously reported two sets {(**1a**, **1b**, **1c**)[7a] and **2a**[7b]} of $Co^{II}Y^{III}$ complexes (Figure 3) that also have distorted octahedral Co^{II} and nine-coordinated Y^{III} centers. The bond parameters observed in the present instance are consistent with these literature precedents.

Magnetic Properties. The thermal variations of $\chi_M T$ (χ_M, the molar magnetic susceptibility; T, the temperature in Kelvin) for the four compounds are very similar. Thus, the $\chi_M T$ is around 3 cm^3 K mol^{-1} at room temperature and monotonically decreases on cooling down to reach 1.84, 1.63, 1.68, and 1.51 cm^3 K mol^{-1} for complexes **1** to **4** at 2 K, respectively (Figure 4). The room temperature values are much higher than expected for isolated S = 3/2 with g = 2.0 (1.875 cm^3 K mol^{-1}) but match with the commonly accepted values for high spin octahedral Co^{II} with spin orbit coupling in the orbitally degenerate ground state $^4T_{1g}$ and distortions of the octahedral coordination sphere.[22] The low temperature values also match with the stabilization of an S_{eff} = 1/2 effective spin with a g_{eff} close to the 4.33 value expected in the absence of distortion.[19] The first magnetization curves at 2 K are represented also in Figure 4. They tend to saturate at values close to 2.2 Nβ for all compounds in agreement with the expected value of 2.165 Nβ for the effective spin 1/2 with g = 4.33.

To extract the spin Hamiltonian (SH) parameters of all the four complexes, we fitted both the $\chi_M T(T)$ and the $M(H)$ data using PHI software.[23] The following Hamiltonian is used for fitting the data:

$$H = D\left[S_z^2 - \frac{S(S+1)}{3}\right] + E(S_x^2 - S_y^2) + g\mu_B HS$$

DOI: 10.1021/acs.inorgchem.9b00864
Inorg. Chem. 2019, 58, 10725−10735

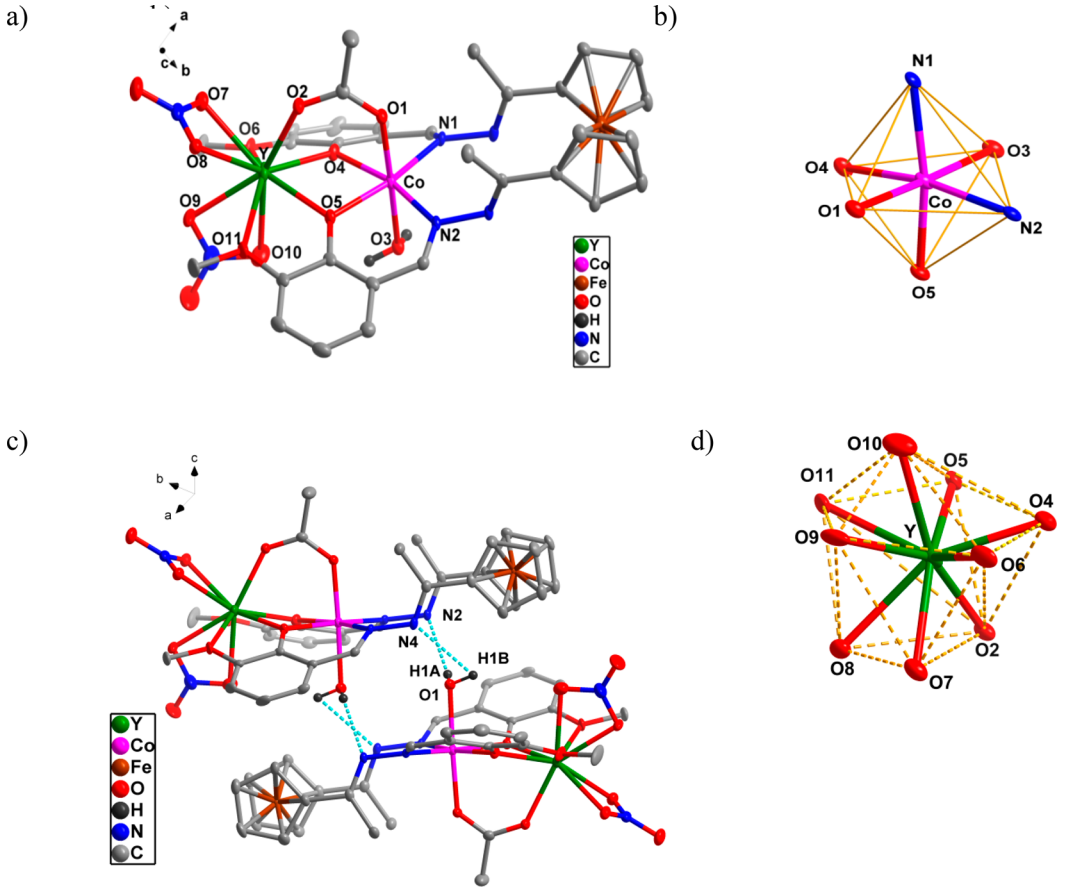

Figure 2. (a) Full molecular structure of **2** (selected hydrogen atoms and solvent molecules are removed for the sake of clarity); (b) distorted octahedral geometry around the Co^{II} ion; (c) two molecules of complex **2** showing intermolecular hydrogen bonding (light blue colored dotted bonds); (d) coordination environment around the Y^{III} ion. (Ellipsoids are drawn at 40% probability for nonmetallic atoms and at 50% probability for metallic atoms.)

Table 1. CShM Values Obtained from Continuous SHAPE Analysis for Complex 1−4

complex	complex **1**	complex **2**	complex **3**	complex **4**
CShM value for the OC-6 polyhedron	0.758	0.763	0.800	0.859

Here, g is the g matrix, μ_B is the Bohr magneton, H is the external magnetic field, S_x, S_y, S_z are the x, y, and z-component of the total spin S respectively. The best tried fit produced D = 87.9 cm^{-1} and E = 11.6 cm^{-1} with g_x, g_y, and g_z = 2.917, 2.334, and 1.855, respectively, for **2**. And for the other three compounds, **1**, **3**, and **4**, the fitted plots and extracted parameters are provided in Figure S7 and in Table S11, respectively.

None of the four compounds display an out-of-phase signal of the ac magnetic susceptibility, χ_M'', in the absence of an external dc field down to 2 K in the frequency range ν = 1 → 10 000 Hz of the oscillating field because of possible quantum tunneling of the magnetization (QTM). However, such a QTM can be suppressed by the application of a moderate external dc field inducing a slowing down of the relaxation of the magnetic moment of Co^{II}. It is characterized by the appearance of a maximum on the χ_M'' vs ν curves between 100 and 1000 Hz for complexes **1**, **3**, and **4**, while the maximum is located at higher frequency (>1000 Hz) for **2** (Figure S9). It is not the only major difference between the four compounds.

Table 2. Selected Bond Parameters for 1−4

bond/angle description	complex **1**	complex **2**	complex **3**	complex **4**
Co−O1	2.099(64)	2.032(23)	2.073(49)	2.067(26)
Co−O3	2.111(64)	2.123(24)	2.153(55)	2.125(29)
Co−O4	2.071(47)	2.061(23)	2.075(51)	2.082(2)
Co−O5	2.079(5)	2.083(22)	2.062(56)	2.069(2)
Co−N1	2.135(69)	2.162(25)	2.136(73)	2.138(27)
Co−N2	2.124(64)	2.109(26)	2.137(71)	2.147(23)
O1−Co−O3	176.294(22)	177.093(94)	177.426(2)	177.946(98)
O1−Co−O4	88.866(21)	88.826(92)	90.461(2)	89.624(92)
O1−Co−O5	88.386(22)	89.017(9)	88.325(2)	88.938(88)

DOI: 10.1021/acs.inorgchem.9b00864
Inorg. Chem. 2019, 58, 10725−10735

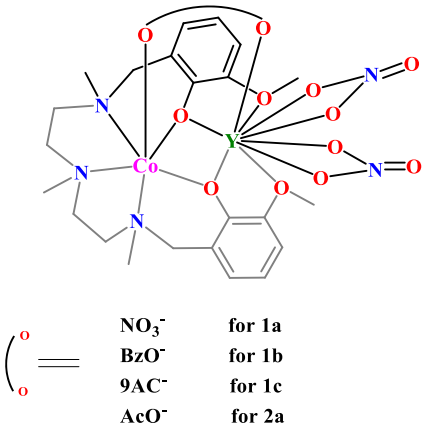

Figure 3. Compounds **1a**, **1b**, **1c**, and **2b** known in the literature.[7]

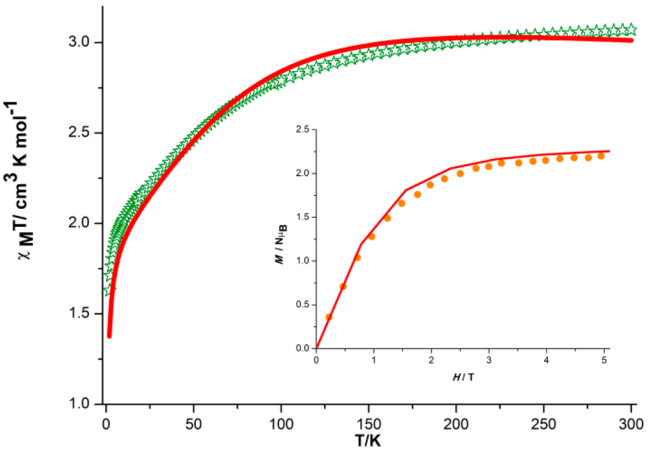

Figure 4. Thermal variation of $\chi_M T$ with the first magnetization curves at 2 K for **2** in the inset. The solid red lines represent the fits obtained for the experimental magnetic data using the parameters described in the main text using PHI software.

Indeed, for **1**, a "so-called" optimum field (the field for which the relaxation is the slowest) is clearly visible around 1200 Oe with an amount of relaxing matter (the amplitude of χ_M'' near the maximum) almost constant above 500 Oe, while for **3** and **4** the relaxation accelerates continuously with the field and the amplitude of χ_M'' increases. Complex **2** seems to behave similarly to **3** and **4** with, however, the maximum, which potentially falls at higher frequencies than 1000 Hz.

The four complexes were studied under an applied magnetic field of 1200 Oe. All the compounds displayed strong frequency dependence of the magnetic susceptibility between 2 and 15 K (Figures 5 and S9).

The AC data for **1**−**3** were fit in the framework of the extended Debye model[24,25] for a single relaxation process with a distribution (α) of relaxation times (τ; Tables S1−S3), while for **4** the frequency maxima are manually selected due to the large out-of-phase signal of the magnetization at low temperature (Figure 5d). The high temperature part of the $\log(\tau)$ versus T curves seems to follow the Arrhenius law $\tau = \tau_0 \exp(\Delta/kT)$ with $\tau_0 = 3.2(4) \times 10^{-6}$ s and $\Delta = 8.4(6)$ K for **1**, $\tau_0 = 2.5(2) \times 10^{-6}$ s and $\Delta = 11.0(4)$ K for **2**, $\tau_0 = 2.6(4) \times 10^{-6}$ s and $\Delta = 13.7(8)$ K for **3**, and $\tau_0 = 7.4(9) \times 10^{-7}$ s and $\Delta = 18.7(6)$ K for **4** (Figure S9). The thermal dependence plots of the relaxation time clearly show a deviation from the linearity below 4 K, a sign of other operative relaxation

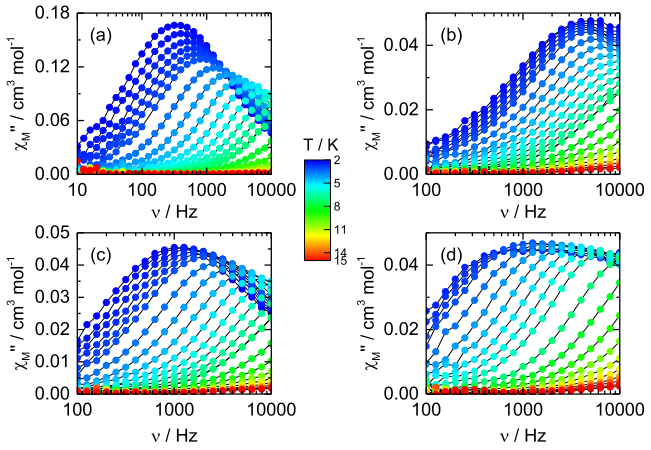

Figure 5. Frequency dependence of χ_M'' between 2 and 10 K for compounds **1**−**4** (a to d, respectively) under a 1200 Oe applied magnetic field.

mechanisms. The much lower experimental energy barrier of the four complexes compared to the calculated values (301.1, 256.2, 303.6, and 222.6 K respectively for **1**−**4** compounds) is an indication of a negligible contribution of the Orbach process with respect to Raman, QTM, and Direct relaxations. Magnetic relaxation through the Direct mechanism can be observed on the scan field of the magnetic susceptibility for **2** and **3** since increasing the magnetic field value induced a shift to the χ_M'' maxima at higher frequency (Figure S8). Therefore, the $\log(\tau)$ versus T curves (Figure 6) in 2−6 K can be analyzed using the following expression:

$$t^{-1} = ATH^4 + CT^n + \tau_{TI}^{-1}$$

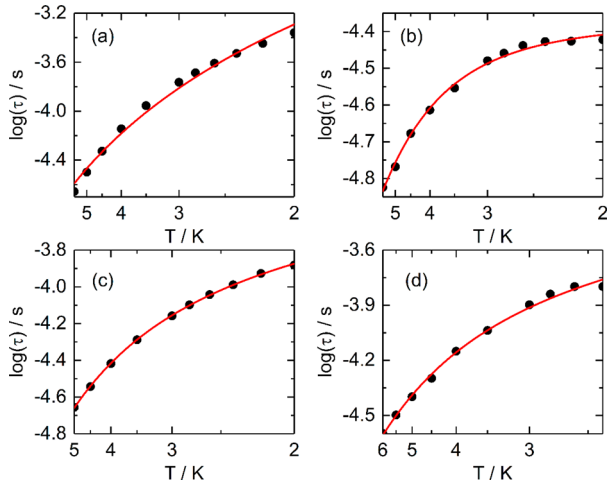

Figure 6. Arrhenius plots of the relaxation times in 1200 Oe applied magnetic field for **1**−**4** (a to d, respectively; black disks). Full red lines are the best-fit curves (see text).

The best fit for compounds **2** and **3** were obtained using the combination of Raman and Direct processes as reported by Colacio[7a] for similar type $Co^{II}Y^{III}$ compounds with the parameters depicted in Table 3. In contrast, the best fit for **4** was obtained by the combination of Raman and remaining QTM, while **1** was obtained using a pure Raman process (Table 3). For the latter, the absence of QTM is explained by the AC measurements under the optimal field of 1200 Oe,

DOI: 10.1021/acs.inorgchem.9b00864
Inorg. Chem. 2019, 58, 10725−10735

Table 3. Fitting Parameters with Associated Errors Given in Brackets for 1−4

	1	2	3	4
C (s^{-1} K^{-n})	252 (30)	90 (16)	37 (29)	154 (51)
n	2.96(10)	3.6(1)	3.7(4)	3.06(19)
τ_{QTM} (s)				2.74(37)×10^{-4}
A (s^{-1} K^{-m}) m fixed to 4		1.54(4) × 10^{-9}	9.6(10) × 10^{-10}	

while for **2**−**4** the optimal magnetic field value cannot be reached.

The extracted values for the n parameter are in agreement with those expected for Kramers ions when both optical and acoustic phonons (n = 1−6) are involved in the relaxation mechanism.[26] As a consequence, **1** is the slowest and **2** is the fastest with **4** and **3** the intermediates.

Theoretical Studies. To illustrate various experimental observations and also to probe the origin of the slow relaxation in the presence of a field, we have undertaken a detailed *ab initio* calculation using two approaches (see computational details for further information). The computed spin Hamiltonian parameters are given in Table 4, and the estimated values are in general agreement with the values obtained from experiments. The estimated axial (rhombic) ZFS parameters, $D(E)$, are given in Table 4 for complexes **1**−**4**. The E/D values are significant, and this corroborates well with larger E values. The values obtained from NEVPT2 calculations are very similar to the values obtained from CASSCF and also using MOLCAS (see Table 4; in the Supporting Information, also see Figure S12 and S13 for computed D orientation with respect to the molecular framework). Positive D obtained for all complexes is in agreement with the experiments where relaxation is observed only in the presence of an applied field.[4,27] Additionally, such a large computed D value suggests that the system can be described using a pseudo-spin 1/2 system. Using a pseudo-spin of 1/2, estimates of the low temperature limit of $\chi_M T$ can be calculated: 2.06, 2.02, 2.12, and 1.88 cm^3 K mol^{-1} for **1** to **4**, respectively. These values are in relatively good agreement with the experiment and corroborated by the saturation values of the magnetization recorded at 2 K, which match the expected 2.2, 2.18, 2.07, and 2.13 Nβ for **1** to **4**, respectively. Additionally, we have simulated the susceptibility and the magnetization data for these complexes using the *ab initio* estimated parameters, and a very good match has been found, which offers confidence in the estimated parameters.

The ground state electronic configuration for the Co^{II} ion is found to be strongly multideterminantal in characteristics for all four complexes. For example, in complex **2**, the ground state has a $(d_{xz})^2(d_{xy})^1(d_{yz})^2(d_{x^2-y^2})^1(d_{z^2})^1$ configuration that is dominant (36%) and is mixed strongly with two other states with a weightage of 20% (See Figure 7). This is expected for the six-coordinate Co^{II} possessing unquenched orbital contribution, leading to larger D values. The dominant contribution to the positive D value is found to arise from the two close lying quartet states, particularly the first quartet state is found to contribute more than 50% to the net D value for all four complexes. The first excited state is also found to be multideterminantal in character with strong mixing and transition from the $d_{xz} \rightarrow d_{xy}$ orbital found to contribute significantly to the total D value. As the two orbitals involved have different m_l levels, the sign of D is found to be positive for all four complexes.[28]

Since the first excited state contributes significantly to the D value, the gap between the ground to the first excited state is strongly correlated to the magnitude of the D value. The trend in the computed D is found to be **2** > **3** > **1** > **4** with the D value computed for complex **4** found to be smaller than the other three complexes. The magnitude of the computed D is found to correlate with the ground to first and second excited states, which are the dominant contributors to the D value. The energies computed for the first and second excited states along with their contribution to the D values are given in Figure 8 and the Supporting Information. Particularly for complex **4**, both the first and second excited quartet states are strongly destabilized compared to complexes **1**−**3**, leading to a smaller D value.

The computed g tensors for complexes **1**−**4** are given in Table 4. Clearly, as we expected for a positive D value, the g_{xx} values are found to be much larger than g_{zz}. Due to the low symmetry of the complexes, the g_{zz} and D_{zz} axes are found to be noncoincident for these complexes (see Figures 9 and S12 and S13). This low symmetry leads to significant E values for all four complexes, and this is reflected in the E/D value, where a high value indicates the rhombic nature of the transverse anisotropy, leading to noncoincidence of the D_{zz} and g_{zz} axes.

The $d_{xz} \rightarrow d_{xy}$ transition is the prime contributor to the positive D, and the computed trend for the magnitude of D among complexes **1**−**4** is also reflected in the contribution arising from the first excited state (i.e., **2** > **3** > **1** > **4**). Qualitatively, the first excited state reflects the energy gap between the d_{xz} and d_{xy} orbitals. Since the d_{xy} orbital is orthogonal to the acetate bridge, its energy is expected to be only marginally influenced by the substitution in the acetate group; however, the energy of the d_{xz} orbital is significantly influenced, as this orbital has a weak π^* antibonding interaction with the acetate oxygen atom. The substitution at the acetate position tends to stabilize or destabilize the d_{xz} orbital, leading to a variation in the d_{xz} to d_{xy} gap and hence the variation in the magnitude of D value among complexes **1**−**4**.

EPR Studies. To have a clear idea on the sign of D, we have recorded Q-band EPR spectra of these complexes on powder samples of **2**−**4** (Figure S15). All the recorded EPR spectra were characteristics of high spin Co^{II} (S = 3/2) with a very high positive ZFS parameter D, as no transitions were observed

Table 4. Estimated D, E, and g Tensors for 1−4 Using *ab Initio* Calculations

	CASSCF/RASSI-SO					NEVPT2				
complexes	D_{cal} (cm^{-1})	E_{cal} (cm^{-1})	g_x	g_y	g_z	D_{cal} (cm^{-1})	E_{cal} (cm^{-1})	g_x	g_y	g_z
1	101.9	13.7	7.075	3.105	2.178	87.9	11.6	6.17	4.745	2.306
2	88.8	3.5	6.984	3.227	2.198	91.7	23.0	5.905	4.979	2.222
3	93.8	27.9	7.296	2.932	2.026	90.0	18.5	7.402	3.042	1.965
4	76.8	5.4	7.218	2.881	1.955	72.4	18.3	5.783	4.597	2.382

DOI: 10.1021/acs.inorgchem.9b00864
Inorg. Chem. 2019, 58, 10725−10735

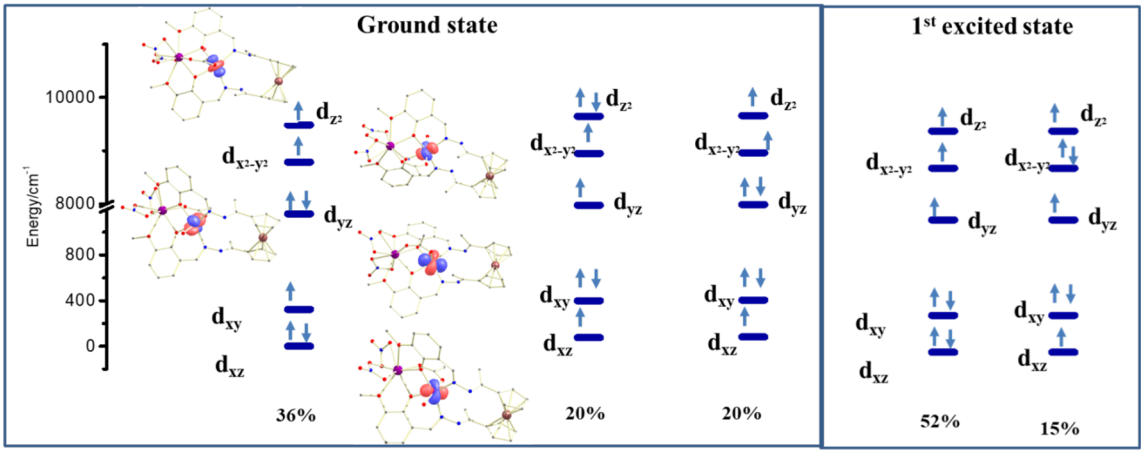

Figure 7. Orbital energies computed for the ground and first excited state of complex **2**. The percentage mention reveals the percent of the corresponding configuration mixing.

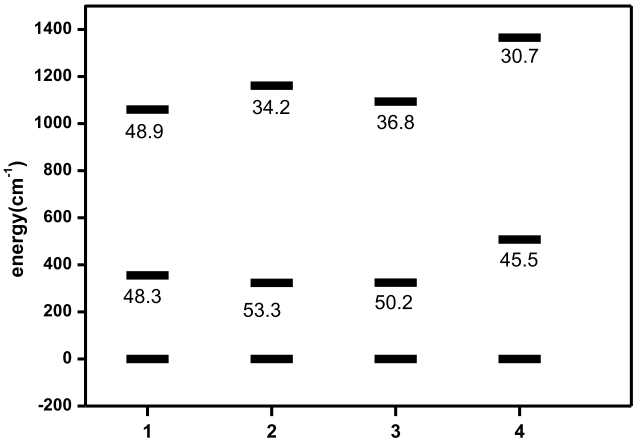

Figure 8. Energy gap between the ground, first and second excited quartet states computed for complexes **1**−**4**. The numbers mentioned below the line reveal the contribution to the *D* value by that particular state (in cm^{-1}).

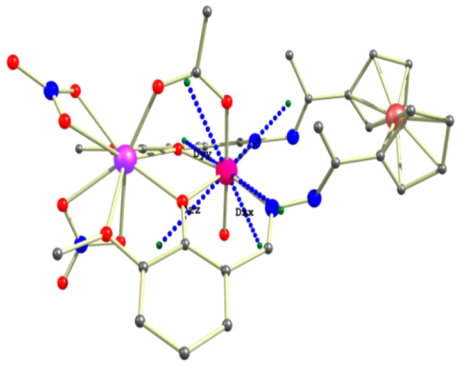

Figure 9. Computed orientation of D_{zz} and g_{zz} axes for complex **2**.

for $m_s = \pm 1/2$ to $m_s = \pm 3/2$ levels since the energy gap between the two levels is much higher (consistent with values obtained from the CASSCF and NEVPT2 results, 150 cm^{-1} to 210 cm^{-1}) and validates the pseudospin approximation that was adapted as discussed earlier. The recorded EPR spectra are very similar to the EPR data reported earlier for the octahedral Co^{II} complexes possessing positive *D* and offer confidence in the estimated parameters.[7]

The observed transition could be attributed to the transition between the $m_s = \pm 1/2$ levels, hence, the $m_s = \pm 1/2$ is the ground state suggesting positive *D*. For the $D < 0$ case, the low lying state is KD = ±3/2 and the transition within these states are generally less visible in the recorded frequency, leading to the absence of any features in the EPR spectra.[7]

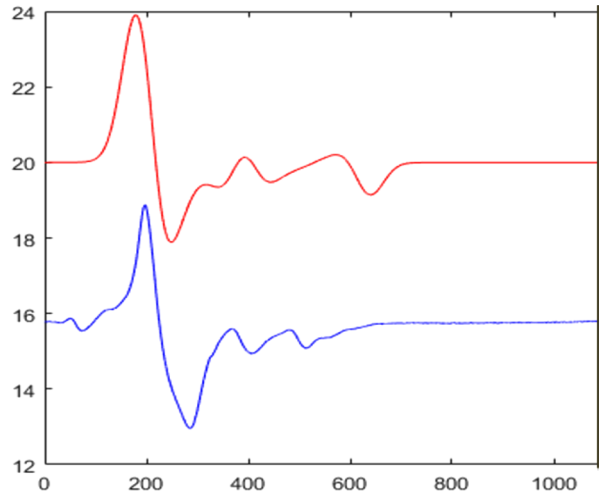

Figure 10. Experimental and simulated Q-band EPR spectra for complex **3** (blue = experimental, red = simulated). Simulation is performed using the following set of spin Hamiltonian parameter D = 93 cm^{-1}, E/D = 0.3, g_{xx} = 4.8, g_{yy} = 2.93, g_{zz} = 1.8, and line width 65.

To further understand the nature of the EPR spectra, we have simulated the EPR spectra of complex **3** using NEVPT2 estimated *D*, *E*, and *g* values and with minor perturbations to the *g* tensors (Figure 10). Many of the experimental features are reproducible, offering confidence in the sign of the assigned *D*.

CONCLUSION

A complete and proper understanding of the relation between geometric and electronic structure with magnetic properties in metal complexes in general and in 3d/4f complexes in particular is still an incompletely fulfilled objective and demands continuous experimental and theoretical work. In this regard, with an objective to understand some of the

DOI: 10.1021/acs.inorgchem.9b00864
Inorg. Chem. 2019, 58, 10725−10735

features underlying the magnetic properties in Co^{II} complexes, we have chosen to examine heterometallic $Co^{II}Y^{III}$ systems since Y^{III} is a diamagnetic ion. We have synthesized four complexes in a targeted way by altering carboxylate bridging ligands. We explored to understand how the electronic properties of the bridging carboxylate ligands in the $Co^{II}Y^{III}$ systems control the magnetic anisotropy as well as the magnetic slow relaxation. The six coordinated distorted octahedral geometry around the Co^{II} center within the molecules dictates that the molecule show a field induced magnetic relaxation. The extracted energy barriers for the high temperature region for the molecules are seen to be dependent on the nature of the bridging ligand. Ab initio calculation showed that all the molecules have positive D values, which is largely due to the contribution of the transition from d_{xz} to d_{xy} orbitals for the molecules. Also, it was calculated that although the effect of bridging ligand on the d_{xy} orbital is not so prominent, the d_{xz} orbital is in direct interaction with the π^* orbital of the O atoms of the bridging ligand. Thus, subtle changes in the electronic properties on the bridging ligands stabilize or destabilize the d_{xz} orbital, leading to a variation in the magnitude of the D value for the complexes **1**−**4**. This has a direct bearing on the slow relaxation of magnetization in these complexes. Further work in this field could include the use of other types of ligands, including those involving sulfur/carbenes which are expected to influence directly the crystal field around the metal ion and in turn the magnetic properties. Such studies are underway in our laboratory.

■ ASSOCIATED CONTENT

Supporting Information

The Supporting Information is available free of charge on the ACS Publications website at DOI: 10.1021/acs.inorgchem.9b00864.

> Crystallographic table, mass spectra of the complexes, crystal packing diagrams; NEVPT2 calculated parameters, further description of PHI fitting, and *ab initio* calculation on the compounds (PDF)

Accession Codes

CCDC 1904649−1904652 contain the supplementary crystallographic data for this paper. These data can be obtained free of charge via www.ccdc.cam.ac.uk/data_request/cif, or by emailing data_request@ccdc.cam.ac.uk, or by contacting The Cambridge Crystallographic Data Centre, 12 Union Road, Cambridge CB2 1EZ, UK; fax: +44 1223 336033.

■ AUTHOR INFORMATION

Corresponding Authors

*E-mail: vc@iitk.ac.in.
*E-mail: rajaraman@chem.iitb.ac.in.
*E-mail: fabrice.pointillart@univ-rennes1.fr.

ORCID

Joydev Acharya: 0000-0002-9480-4725
Fabrice Pointillart: 0000-0001-7601-1927
Gopalan Rajaraman: 0000-0001-6133-3026
Vadapalli Chandrasekhar: 0000-0003-1968-2980

Notes

The authors declare no competing financial interest.

■ ACKNOWLEDGMENTS

We thank the Department of Science and Technology (DST), India; the CNRS, Université de Rennes 1, the European Commission through the ERC-CoG 725184 MULTIPROSMM (project no. 725184) for financial support, and also support for the Single Crystal CCD X-ray Diffractometer facility at IIT-Kanpur. V.C. is grateful to the DST for a J. C. Bose fellowship. J.A. thanks Department of Science and Technology (DST), India for INSPIRE Senior Research Fellowship. J.A. is also thankful to Mr. Arup Sarkar, IITB, for discussion and help. G.R. would like to thank SERB for funding (CRG/2018/000430) and the IITB multifrequency EPR facility for recording the EPR spectra.

■ REFERENCES

(1) (a) Hill, S.; Edwards, R. S.; Aliaga-Alcalde, N.; Christou, G. Quantum Coherence in an Exchange-Coupled Dimer of Single-Molecule Magnets. *Science* **2003**, *302*, 1015−1018. (b) Leuenberger, M. N.; Loss, D. Quantum computing in molecular magnets. *Nature* **2001**, *410*, 789−793.

(2) (a) Craig, G. A.; Sarkar, A.; Woodall, C. H.; Hay, M. A.; Marriott, K. E. R.; Kamenev, K. V.; Moggach, S. A.; Brechin, E. K.; Parsons, S.; Rajaraman, G.; Murrie, M. Probing the origin of the giant magnetic anisotropy in trigonal bipyramidal Ni(ii) under high pressure. *Chem. Sci.* **2018**, *9*, 1551−1559. (b) El-Khatib, F.; Cahier, B.; López-Jordà, M.; Guillot, R.; Rivière, E.; Hafez, H.; Saad, Z.; Girerd, J.-J.; Guihéry, N.; Mallah, T. Design of a Binuclear Ni(II) Complex with Large Ising-type Anisotropy and Weak Anti-Ferromagnetic Coupling. *Inorg. Chem.* **2017**, *56*, 10655−10663. (c) Freedman, D. E.; Harman, W. H.; Harris, T. D.; Long, G. J.; Chang, C. J.; Long, J. R. Slow Magnetic Relaxation in a High-Spin Iron(II) Complex. *J. Am. Chem. Soc.* **2010**, *132*, 1224−1225. (d) Novikov, V. V.; Pavlov, A. A.; Nelyubina, Y. V.; Boulon, M.-E.; Varzatskii, O. A.; Voloshin, Y. Z.; Winpenny, R. E. P. A Trigonal Prismatic Mononuclear Cobalt(II) Complex Showing Single-Molecule Magnet Behavior. *J. Am. Chem. Soc.* **2015**, *137*, 9792−9795. (e) Rechkemmer, Y.; Breitgoff, F. D.; van der Meer, M.; Atanasov, M.; Hakl, M.; Orlita, M.; Neugebauer, P.; Neese, F.; Sarkar, B.; van Slageren, J. A four-coordinate cobalt(II) single-ion magnet with coercivity and a very high energy barrier. *Nat. Commun.* **2016**, *7*, 10467−10474. (f) Shao, F.; Cahier, B.; Rivière, E.; Guillot, R.; Guihéry, N.; Campbell, V. E.; Mallah, T. Structural Dependence of the Ising-type Magnetic Anisotropy and of the Relaxation Time in Mononuclear Trigonal Bipyramidal Co(II) Single Molecule Magnets. *Inorg. Chem.* **2017**, *56*, 1104−1111. (g) Vaidya, S.; Tewary, S.; Singh, S. K.; Langley, S. K.; Murray, K. S.; Lan, Y.; Wernsdorfer, W.; Rajaraman, G.; Shanmugam, M. What Controls the Sign and Magnitude of Magnetic Anisotropy in Tetrahedral Cobalt(II) Single-Ion Magnets? *Inorg. Chem.* **2016**, *55*, 9564−9578. (h) Zadrozny, J. M.; Xiao, D. J.; Atanasov, M.; Long, G. J.; Grandjean, F.; Neese, F.; Long, J. R. Magnetic blocking in a linear iron(I) complex. *Nat. Chem.* **2013**, *5*, 577−581. (i) Bunting, P. C.; Atanasov, M.; Damgaard-Møller, E.; Perfetti, M.; Crassee, I.; Orlita, M.; Overgaard, J.; van Slageren, J.; Neese, F.; Long, J. R. A linear cobalt(II) complex with maximal orbital angular momentum from a non-Aufbau ground state. *Science* **2018**, *362*, No. eaat7319.

(3) (a) Díaz-Torres, R.; Menelaou, M.; Roubeau, O.; Sorrenti, A.; Brandariz-De-Pedro, G.; Sañudo, E. C.; Teat, S. J.; Fraxedas, J.; Ruiz, E.; Aliaga-Alcalde, N. Multiscale study of mononuclear CoII SMMs based on curcuminoid ligands. *Chem. Sci.* **2016**, *7*, 2793−2803. (b) Herchel, R.; Váhovská, L.; Potočnák, I.; Trávníček, Z. Slow Magnetic Relaxation in Octahedral Cobalt(II) Field-Induced Single-Ion Magnet with Positive Axial and Large Rhombic Anisotropy. *Inorg. Chem.* **2014**, *53*, 5896−5898. (c) Korchagin, D. V.; Palii, A. V.; Yureva, E. A.; Akimov, A. V.; Misochko, E. Y.; Shilov, G. V.; Talantsev, A. D.; Morgunov, R. B.; Shakin, A. A.; Aldoshin, S. M.; Tsukerblat, B. S. Evidence of field induced slow magnetic relaxation in

DOI: 10.1021/acs.inorgchem.9b00864
Inorg. Chem. 2019, 58, 10725−10735

cis-[Co(hfac)$_2$(H$_2$O)$_2$] exhibiting tri-axial anisotropy with a negative axial component. *Dalton Trans.* **2017**, *46*, 7540−7548. (d) Palii, A. V.; Korchagin, D. V.; Yureva, E. A.; Akimov, A. V.; Misochko, E. Y.; Shilov, G. V.; Talantsev, A. D.; Morgunov, R. B.; Aldoshin, S. M.; Tsukerblat, B. S. Single-Ion Magnet Et$_4$N[Co^{II}(hfac)$_3$] with Nonuniaxial Anisotropy: Synthesis, Experimental Characterization, and Theoretical Modeling. *Inorg. Chem.* **2016**, *55*, 9696−9706. (e) Sertphon, D.; Murray, K. S.; Phonsri, W.; Jover, J.; Ruiz, E.; Telfer, S. G.; Alkaş, A.; Harding, P.; Harding, D. J. Slow relaxation of magnetization in a bis-mer-tridentate octahedral Co(ii) complex. *Dalton Trans.* **2018**, *47*, 859−867. (f) Vallejo, J.; Castro, I.; Ruiz-García, R.; Cano, J.; Julve, M.; Lloret, F.; De Munno, G.; Wernsdorfer, W.; Pardo, E. Field-Induced Slow Magnetic Relaxation in a Six-Coordinate Mononuclear Cobalt(II) Complex with a Positive Anisotropy. *J. Am. Chem. Soc.* **2012**, *134*, 15704−15707.

(4) Gómez-Coca, S.; Urtizberea, A.; Cremades, E.; Alonso, P. J.; Camón, A.; Ruiz, E.; Luis, F. Origin of slow magnetic relaxation in Kramers ions with non-uniaxial anisotropy. *Nat. Commun.* **2014**, *5*, 4300−4307.

(5) Chandrasekhar, V.; Pandian, B. M.; Azhakar, R.; Vittal, J. J.; Clérac, R. Linear Trinuclear Mixed-Metal Co^{II}-Gd^{III}-Co^{II} Single-Molecule Magnet: [L$_2$Co$_2$Gd][NO$_3$]·2CHCl$_3$ (LH$_3$ = (S)P[N(Me)-NCH-C$_6$H$_3$-2-OH-3-OMe]$_3$). *Inorg. Chem.* **2007**, *46*, 5140−5142.

(6) (a) Gómez, V.; Vendier, L.; Corbella, M.; Costes, J.-P. Tetranuclear [Co-Gd]$_2$ Complexes: Aiming at a Better Understanding of the 3d-Gd Magnetic Interaction. *Inorg. Chem.* **2012**, *51*, 6396−6404. (b) Goura, J.; Chakraborty, A.; Walsh, J. P. S.; Tuna, F.; Chandrasekhar, V. Hexanuclear 3d-4f Neutral Co$^{II}_2$Ln$^{III}_4$ Clusters: Synthesis, Structure, and Magnetism. *Cryst. Growth Des.* **2015**, *15*, 3157−3165. (c) Modak, R.; Sikdar, Y.; Thuijs, A. E.; Christou, G.; Goswami, S. Co$^{II}_4$, Co$^{II}_7$, and a Series of Co$^{II}_2$Ln^{III} (Ln^{III} = Nd^{III}, Sm^{III}, Gd^{III}, Tb^{III}, Dy^{III}) Coordination Clusters: Search for Single Molecule Magnets. *Inorg. Chem.* **2016**, *55*, 10192−10202. (d) Radu, I.; Kravtsov, V. C.; Ostrovsky, S. M.; Reu, O. S.; Krämer, K.; Decurtins, S.; Liu, S.-X.; Klokishner, S. I.; Baca, S. G. Tetranuclear {Co$^{II}_2$Co$^{III}_2$}, Octanuclear {Co$^{II}_4$Co$^{III}_4$}, and Hexanuclear {Co$^{III}_3$Dy$^{III}_3$} Pivalate Clusters: Synthesis, Magnetic Characterization, and Theoretical Modeling. *Inorg. Chem.* **2017**, *56*, 2662−2676. (e) Reu, O.; Palii, A.; Ostrovsky, S.; Wallace, W.; Zaharko, O.; Chandrasekhar, V.; Clerac, R.; Klokishner, S. Experimental Characterization and Theoretical Modeling of a Linear [Co$^{II}_2$Tb^{III}] Single Molecule Magnet. *J. Phys. Chem. C* **2013**, *117*, 6880−6888.

(7) (a) Palacios, M. A.; Nehrkorn, J.; Suturina, E. A.; Ruiz, E.; Gómez-Coca, S.; Holldack, K.; Schnegg, A.; Krzystek, J.; Moreno, J. M.; Colacio, E. Analysis of Magnetic Anisotropy and the Role of Magnetic Dilution in Triggering Single-Molecule Magnet (SMM) Behavior in a Family of Co^{II}Y^{III} Dinuclear Complexes with Easy-Plane Anisotropy. *Chem. - Eur. J.* **2017**, *23*, 11649−11661. (b) Colacio, E.; Ruiz, J.; Ruiz, E.; Cremades, E.; Krzystek, J.; Carretta, S.; Cano, J.; Guidi, T.; Wernsdorfer, W.; Brechin, E. K. Slow Magnetic Relaxation in a Co^{II}-Y^{III} Single-Ion Magnet with Positive Axial Zero-Field Splitting. *Angew. Chem., Int. Ed.* **2013**, *52*, 9130−9134.

(8) (a) Xue, S.; Guo, Y.-N.; Ungur, L.; Tang, J.; Chibotaru, L. F. Tuning the Magnetic Interactions and Relaxation Dynamics of Dy$_2$ Single-Molecule Magnets. *Chem. - Eur. J.* **2015**, *21*, 14099−14106. (b) Upadhyay, A.; Das, C.; Vaidya, S.; Singh, S. K.; Gupta, T.; Mondol, R.; Langley, S. K.; Murray, K. S.; Rajaraman, G.; Shanmugam, M. Role of the Diamagnetic Zinc(II) Ion in Determining the Electronic Structure of Lanthanide Single-Ion Magnets. *Chem. - Eur. J.* **2017**, *23*, 4903−4916. (c) Burrow, C. E.; Burchell, T. J.; Lin, P.-H.; Habib, F.; Wernsdorfer, W.; Clérac, R.; Murugesu, M. Salen-Based [Zn$_2$Ln$_3$] Complexes with Fluorescence and Single-Molecule-Magnet Properties. *Inorg. Chem.* **2009**, *48*, 8051−8053. (d) Chakraborty, A.; Goura, J.; Kalita, P.; Swain, A.; Rajaraman, G.; Chandrasekhar, V. Heterometallic 3d-4f single molecule magnets containing diamagnetic metal ions. *Dalton Trans.* **2018**, *47*, 8841−8864. (e) Li, J.; Wei, R.-M.; Pu, T.-C.; Cao, F.; Yang, L.; Han, Y.; Zhang, Y.-Q.; Zuo, J.-L.; Song, Y. Tuning quantum tunnelling of magnetization through 3d-4f magnetic interactions: an alternative approach for manipulating single-molecule magnetism. *Inorg. Chem. Front.* **2017**, *4*, 114−122. (f) Oyarzabal, I.; Artetxe, B.; Rodríguez-Diéguez, A.; García, J. Á.; Seco, J. M.; Colacio, E. A family of acetato-diphenoxo triply bridged dimetallic Zn^{II}Ln^{III} complexes: SMM behavior and luminescent properties. *Dalton Trans.* **2016**, *45*, 9712−9726. (g) Ruiz, J.; Lorusso, G.; Evangelisti, M.; Brechin, E. K.; Pope, S. J. A.; Colacio, E. Closely-Related Zn$^{II}_2$Ln$^{III}_2$ Complexes (Ln^{III} = Gd, Yb) with Either Magnetic Refrigerant or Luminescent Single-Molecule Magnet Properties. *Inorg. Chem.* **2014**, *53*, 3586−3594.

(9) (a) Chandrasekhar, V.; Dey, A.; Mota, A. J.; Colacio, E. Slow Magnetic Relaxation in Co(III)-Co(II) Mixed-Valence Dinuclear Complexes with a Co^{II}O$_5$X (X = Cl, Br, NO$_3$) Distorted-Octahedral Coordination Sphere. *Inorg. Chem.* **2013**, *52*, 4554−4561. (b) Zhu, Y.-Y.; Cui, C.; Zhang, Y.-Q.; Jia, J.-H.; Guo, X.; Gao, C.; Qian, K.; Jiang, S.-D.; Wang, B.-W.; Wang, Z.-M.; Gao, S. Zero-field slow magnetic relaxation from single Co(ii) ion: a transition metal single-molecule magnet with high anisotropy barrier. *Chem. Sci.* **2013**, *4*, 1802−1806.

(10) Chakraborty, A.; Bag, P.; Rivière, E.; Mallah, T.; Chandrasekhar, V. Assembly of heterobimetallic Ni^{II}-Ln^{III} (Ln^{III} = Dy^{III}, Tb^{III}, Gd^{III}, Ho^{III}, Er^{III}, Y^{III}) complexes using a ferrocene ligand: slow relaxation of the magnetization in Dy^{III}, Tb^{III} and Ho^{III} analogues. *Dalton Trans.* **2014**, *43*, 8921−8932.

(11) (a) Vogel, A. I.; Furniss, B. S.; Hannaford, A. J.; Smith, P. W. G.; Tatchell, A. R. *Vogel's Textbook of Practical Organic Chemistry*, 5th ed.; Longman: Harlow, England, 1989. (b) Williams, D. B. G.; Lawton, M. Drying of Organic Solvents: Quantitative Evaluation of the Efficiency of Several Desiccants. *J. Org. Chem.* **2010**, *75*, 8351−8354.

(12) *SMART Software Reference Manual*; *SAINT Software Reference Manual*; Bruker Analytical X-ray Systems, 2003.

(13) Sheldrick, G. M. *SADABS: A software for empirical absorption correction*, Ver. 2.05; University of Göttingen: Göttingen, Germany, 2002.

(14) *SHELXTL Reference Manual*; Bruker Analytical X-ray Systems, Inc.: Madison, WI, 2000.

(15) Sheldrick, G. A short history of SHELX. *Acta Crystallogr., Sect. A: Found. Crystallogr.* **2008**, *64*, 112−122.

(16) Dolomanov, O. V.; Bourhis, L. J.; Gildea, R. J.; Howard, J. A. K.; Puschmann, H. OLEX2: a complete structure solution, refinement and analysis program. *J. Appl. Crystallogr.* **2009**, *42*, 339−341.

(17) Bradenburg, K. *Diamond*, Ver. 3.1eM; Crystal Impact GbR: Bonn, Germany, 2005.

(18) (a) Neese, F. The ORCA program system. *Wiley Interdiscip. Rev. Comput. Mol. Sci.* **2012**, *2*, 73−78. (b) Aquilante, F.; Autschbach, J.; Carlson, R. K.; Chibotaru, L. F.; Delcey, M. G.; De Vico, L.; Fdez. Galvan, I.; Ferre, N.; Frutos, L. M.; Gagliardi, L.; Garavelli, M.; Giussani, A.; Hoyer, C. E.; Li Manni, G.; Lischka, H.; Ma, D.; Malmqvist, P. A.; Muller, T.; Nenov, A.; Olivucci, M.; Pedersen, T. B.; Peng, D.; Plasser, F.; Pritchard, B.; Reiher, M.; Rivalta, I.; Schapiro, I.; Segarra-Marti, J.; Stenrup, M.; Truhlar, D. G.; Ungur, L.; Valentini, A.; Vancoillie, S.; Veryazov, V.; Vysotskiy, V. P.; Weingart, O.; Zapata, F.; Lindh, R. Molcas 8: New capabilities for multiconfigurational quantum chemical calculations across the periodic table. *J. Comput. Chem.* **2016**, *37*, 506−541. (c) Aquilante, F.; De Vico, L.; Ferré, N.; Ghigo, G.; Malmqvist, P.-å.; Neogrády, P.; Pedersen, T. B.; Pitoňák, M.; Reiher, M.; Roos, B. O.; Serrano-Andrés, L.; Urban, M.; Veryazov, V.; Lindh, R. MOLCAS 7: The Next Generation. *J. Comput. Chem.* **2010**, *31*, 224−247. (d) Chibotaru, L. F.; Ungur, L. Ab initio calculation of anisotropic magnetic properties of complexes. I. Unique definition of pseudospin Hamiltonians and their derivation. *J. Chem. Phys.* **2012**, *137*, 064112.

(19) (a) Weigend, F.; Ahlrichs, R. Balanced basis sets of split valence, triple zeta valence and quadruple zeta valence quality for H to Rn: Design and assessment of accuracy. *Phys. Chem. Chem. Phys.* **2005**, *7*, 3297−3305. (b) Maurice, R.; Bastardis, R.; Graaf, C. d.; Suaud, N.; Mallah, T.; Guihéry, N. Universal Theoretical Approach to Extract Anisotropic Spin Hamiltonians. *J. Chem. Theory Comput.* **2009**, *5*, 2977−2984.

DOI: 10.1021/acs.inorgchem.9b00864
Inorg. Chem. 2019, 58, 10725−10735

(20) Roos, B. O.; Lindh, R.; Malmqvist, P.-Å.; Veryazov, V.; Widmark, P.-O.; Borin, A. C. New Relativistic Atomic Natural Orbital Basis Sets for Lanthanide Atoms with Applications to the Ce Diatom and LuF_3. *J. Phys. Chem. A* **2008**, *112*, 11431−11435.
(21) (a) Rouvray, D. H.; Hargittai, I. Book Review: Fuzzy Definitions: Concepts in Chemistry—A Contemporary Challenge. Edited by D. H. Rouvray. *Angew. Chem., Int. Ed. Engl.* **1997**, *36*, 2525. (b) Zabrodsky, H.; Peleg, S.; Avnir, D. Continuous symmetry measures. *J. Am. Chem. Soc.* **1992**, *114*, 7843−7851.
(22) Kahn, O. *Molecular Magnetism*; VCH Publishers: New York, 1993.
(23) Chilton, N. F.; Anderson, R. P.; Turner, L. D.; Soncini, A.; Murray, K. S. PHI: A powerful new program for the analysis of anisotropic monomeric and exchange-coupled polynuclear d- and f-block complexes. *J. Comput. Chem.* **2013**, *34*, 1164−1175.
(24) Dekker, C.; Arts, A. F. M.; de Wijn, H. W.; van Duyneveldt, A. J.; Mydosh, J. A. Activated dynamics in a two-dimensional Ising spin glass: $Rb_2Cu_{1-x}Co_xF_4$. *Phys. Rev. B: Condens. Matter Mater. Phys.* **1989**, *40*, 11243−11251.
(25) Cole, K. S.; Cole, R. H. Dispersion and Absorption in Dielectrics I. Alternating Current Characteristics. *J. Chem. Phys.* **1941**, *9*, 341−351.
(26) Eichhöfer, A.; Lan, Y.; Mereacre, V.; Bodenstein, T.; Weigend, F. Slow Magnetic Relaxation in Trigonal-Planar Mononuclear Fe(II) and Co(II) Bis(trimethylsilyl)amido Complexes—A Comparative Study. *Inorg. Chem.* **2014**, *53*, 1962−1974.
(27) Gomez-Coca, S.; Cremades, E.; Aliaga-Alcalde, N.; Ruiz, E. Mononuclear Single-Molecule Magnets: Tailoring the Magnetic Anisotropy of First-Row Transition-Metal Complexes. *J. Am. Chem. Soc.* **2013**, *135*, 7010−7018.
(28) Chattopadhyay, K.; Heras Ojea, M. J.; Sarkar, A.; Murrie, M.; Rajaraman, G.; Ray, D. Trapping of a Pseudotetrahedral $Co^{II}O_4$ Core in Mixed-Valence Mixed-Geometry $[Co_5]$ Coordination Aggregates: Synthetic Marvel, Structures, and Magnetism. *Inorg. Chem.* **2018**, *57*, 13176−13187.

DOI: 10.1021/acs.inorgchem.9b00864
Inorg. Chem. 2019, 58, 10725−10735